

Additive manufacturing of mechanical testing samples based on virgin poly (lactic acid) (PLA) and PLA/wood fibre composites

Yu Dong¹  · Jamie Milentis¹ · Alokesh Pramanik¹

Received: 4 May 2017 / Accepted: 8 January 2018 / Published online: 9 February 2018
© Shanghai University and Springer-Verlag GmbH Germany, part of Springer Nature 2018

Abstract 3D printing in additive manufacturing is considered as one of key technologies to the future high-precision manufacturing in order to benefit diverse industries in building construction, product development, biomedical innovation, etc. The increasing applications of 3D printed components depend primarily on their significant merits of reduced weight, minimum used materials, high precision and shorter production time. Furthermore, it is very crucial that such 3D printed components can maintain the same or even better material performance and product quality as those achieved by conventional manufacturing methods. This study successfully fabricated 3D printed mechanical testing samples of PLA and PLA/wood fibre composites. 3D printing parameters including infill density, layer height and the number of shells were investigated via design of experiments (DoE), among which the number of shells was determined as the most significant factor for maximising tensile strengths of PLA samples. Further, DoE work evaluated the effect of material type (i.e., neat PLA and PLA/wood fibres) and the number of shells on tensile, flexural and impact strengths of material samples. It is suggested that material type is the only predominant factor for maximising all mechanical strengths, which however are consistently lower for PLA/wood fibre composites when compared with those of neat PLA. Increasing the number of shells, on the other hand, has been found to improve almost all strength levels and decrease infill cavities.

Keywords Additive manufacturing (AM) · Poly (lactic acid) (PLA) · Wood fibres · Polymer composites · Design of experiments (DoEs)

1 Introduction

3D printing is well-known additive manufacturing (AM) to apply materials one layer at a time and produce solid components based on 3D computer-aided design (CAD) models [1, 2]. Components are generally fabricated by dividing the objects of 3D models into thousands of single layers in different ways according to the capability of printing machinery. The key advantage lies in its use as a rapid prototyping tool for product development without expensive tooling, which is essential to conventional manufacturing techniques (e.g., casting and moulding). Consequently, manufacturing cost and commercialisation time can be significantly reduced since new products need less machinery customisation. 3D printing technology has been well positioned in various industries ranging from automotive, aerospace, engineering and medical areas, biological systems to food supply chains [3].

The available 3D printing materials comprise plastics, composites, metals, ceramics, biomaterials and food materials. In particular, acrylonitrile butadiene styrene (ABS), polycarbonates, poly (lactic acid) (PLA), nylon and polyetherimide are among those popular 3D printable plastics. The global drive for more environmentally sustainable materials leads to such a great demand to replace petro-based polymers. PLA is such a biodegradable polymer that is derived naturally from agricultural corns or sugar canes. The close nexus between PLA and 3D printing has been well established in the field of tissue scaffolding, in which cell attachment and proliferation can be achieved

✉ Yu Dong
Y.Dong@curtin.edu.au

¹ Department of Mechanical Engineering, Curtin University, GPO Box U1987, Perth, WA 6845, Australia

in a biological and mechanical environment suitable for tissue regeneration [4]. In order to confirm the viability of 3D printing technology for tissue scaffolds, Patricio et al. [5] investigated a single scaffold made of poly (ϵ -caprolactone) (PCL) and PCL/PLA blends using a new “BioCell printing” process. After the evaluation of resulting scaffold product via scanning electron microscopy, atomic force microscopy and biological characterisation, it was concluded that the used material and method were able to generate the product for cell proliferation and adhesion. Senatov et al. [6] obtained PLA 15% (weight) hydroxyapatite (HA) porous scaffolds by 3D printing using fused filament fabrication. Such scaffolds achieved pore sizes of 700 μm with a porosity of 30%. The shape recovery of scaffolds after deformation was 98%, which suggested their potential use as self-fitting implants for bone replacement. Rosenzweig et al. [7] studied mechanical and biological properties of 3D printed ABS/PLA scaffolds. It was reported that both materials laid out an adequate basis for cell growth and sustained scaffold stability despite being printed from a simplistic and inexpensive desktop printer. On the other hand, 3D printing composite materials is also of great interest to manufacturers and engineers for bioengineering [8, 9] and biomaterials [10, 11], reinforcements for light-weight structures [12], as well as mechanical parts [13]. Bakarich et al. [9] reported the use of additive manufacturing with the combination of digital modelling and 3D printing to fabricate fibre reinforced hydrogel composites. Alginate/acrylamide gel precursor solution and epoxy based UV-curable adhesive were selectively patterned with the aid of an extrusion printer. Such swollen composites were found to demonstrate good agreement with conventional composite theory based on “rule of mixture” for predicting their elastic moduli. Furthermore, their potential application in bioengineering was proven by illustrating a prototyped meniscus cartilage. Le Duigou et al. [10] employed a 3D printing technique to manufacture wood fibre biocomposites and also investigated the effects of printing orientation (i.e., 0° and 90°) and printing width on their mechanical properties. When compared with compressed samples, printed biocomposites possessed much lower Young’s moduli and tensile strengths, which could be associated with highly porous microstructures of printed biocomposites leading to not only damage mechanisms but also water absorption and swelling. Compton and Lewis [12] utilised a new epoxy-based ink to fabricate 3D printed cellular composites with alignment-controlled, multi-scaled and high-aspect-ratio fibre reinforcements. Moreover, these cellular composites with light-weight feature and exceptional mechanical properties enabled to generate hierarchical structures bio-inspired by balsa wood.

Mechanical testing samples of polymers and polymer composites have been widely fabricated in injection

moulding, compression moulding and solution casting processes, which depend primarily on different material characteristics. Nevertheless, the manufacture of testing samples based on 3D printing technology is still limited at the “trial and error” stage. The effect of 3D printing parameters and material selection on their mechanical properties has not been clearly known yet. In this study, the impacts of three key processing parameters, namely infill density, layer height and the number of shells as well as different material types (PLA vs. PLA/wood fibre composites) on tensile, flexural and impact strengths were assessed with a DoE analysis in order to provide a feasible manufacture protocol for the further process optimisation.

2 Materials and experimental setup

PLA and PLA/wood fibre monofilaments (blend ratio: 40:60) with the filament diameter of 1.75 mm were purchased from Bilby 3D, NSW, Australia. As illustrated in Fig. 1a, 3D printing machine used in this study is MakerBot Replicator 2 \times (MakerBot Industries, Brooklyn, NY, USA). All tensile, flexural and impact testing samples were 3D printed at the nozzle temperature of 230 $^\circ\text{C}$ and base plate temperature of 70 $^\circ\text{C}$ with a feed rate of 90 mm/s, (see Fig. 1b).

3 Mechanical testing and material characterisation

Tensile tests were conducted on a Llyod EZ50 universal testing machine with a load cell capacity of 50 kN. 3D printed dog-bone tensile samples (specimen type IV, 115 mm \times 19 mm \times 3.2 mm) were stretched until the fracture occurred at a crosshead speed of 5 mm/min in compliance with ASTM D638 standard.

The same Llyod testing machine (load cell: 10 kN), mounted with a 3-point bending apparatus, was employed for flexural testing 3D printed strip-like samples (127 mm \times 12.7 mm \times 3.2 mm) at 13.653 mm/min with a support span of 51.2 mm based on ASTM 790 standard. Furthermore, Charpy impact tests were carried out by using a Zwick 5102 (model D-7900) impact tester with a 0.5 J hammer and their corresponding samples (the same dimensions as those of flexural samples) were notched with an angle of 45° according to ASTM D6110 standard. The average data were reported based on testing results of at least five samples for each material batch, along with calculated standard deviations to evaluate test reproducibility.

For the fractographic analysis, a Pro-MicroScan microscope with an eyepiece camera (Oplenic Corporation,

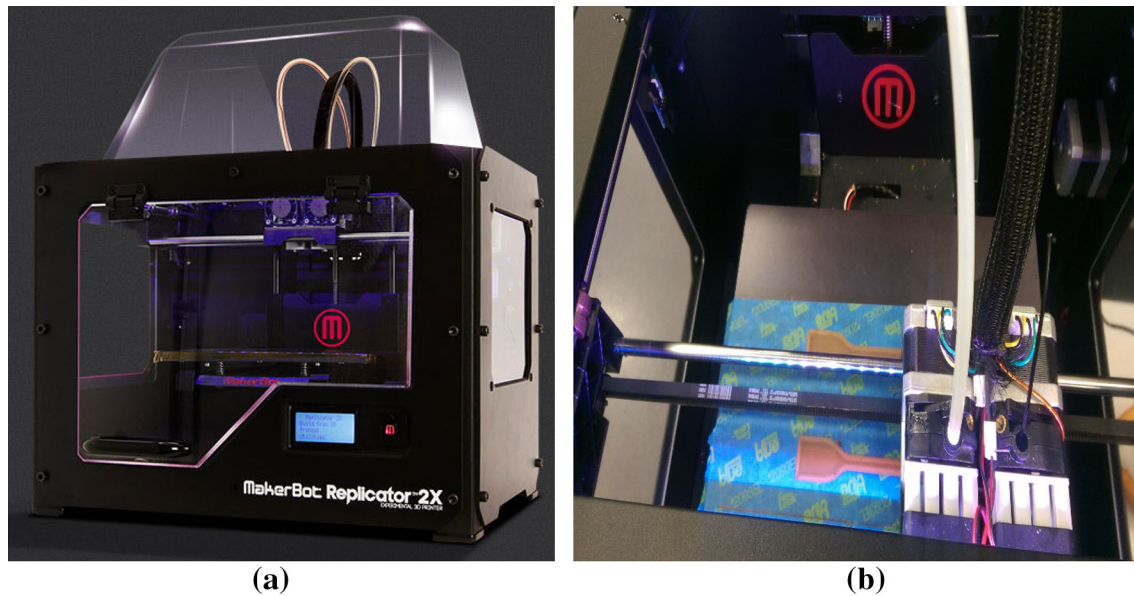


Fig. 1 a Setup of MakerBot Replicator 2× b 3D printing of testing samples using MakerBot Replicator 2×

Table 1 DoE factors and levels for 3D printing neat PLA tensile samples

Factor	Level	
	1	2
A: Infill density /%	15	45
B: Layer height /mm	0.1	0.2
C: Number of shells	2	6

China) was operated to examine fractured cross-sectional structures of testing material samples.

4 DoE array based on key processing parameters

In the initial experimental design, three key processing parameters for 3D printing, namely infill density, layer height and the number of shells, are altered as given in Table 1, in which infill density is 15% (machine default)

and 45%, layer height is 0.1 (machine default) and 0.2 mm and the number of shells consists of 2 and 6 for low and high settings, respectively. As illustrated in Table 2, a typical Taguchi L_8 (2^3) DoE orthogonal array [14] with factorial interactions was utilised to determine significant factors from above-mentioned processing parameters. For simplicity, only 3D printing for neat PLA tensile testing samples was conducted. The DoE response was set to maximise tensile strengths of PLA testing samples based on a “larger-the-better” characteristic [14, 15] given by

$$S/N = -10 \log \left(\frac{1}{n} \sum_{i=1}^n \frac{1}{y_i^2} \right) \quad (1)$$

where S/N is a signal-to-noise ratio for improved quality and measurement with the variability reduction in robust design and manufacturing [14–16]; n is the number of samples in each DoE run and y is measured response for the DoE target (i.e., the maximisation of tensile strength in this case). The noise effect in this DoE study comes from the discrepancy of

Table 2 L_8 orthogonal array for 3D printing neat PLA tensile samples

DoE run	A: Infill density/%	B: Layer height /mm	C: Number of shells	AB	BC	AC	ABC
1	1	1	1	1	1	1	1
2	1	1	2	1	2	2	2
3	1	2	1	2	2	1	2
4	1	2	2	2	1	2	1
5	2	1	1	2	1	2	2
6	2	1	2	2	2	1	1
7	2	2	1	1	2	2	1
8	2	2	2	1	1	1	2

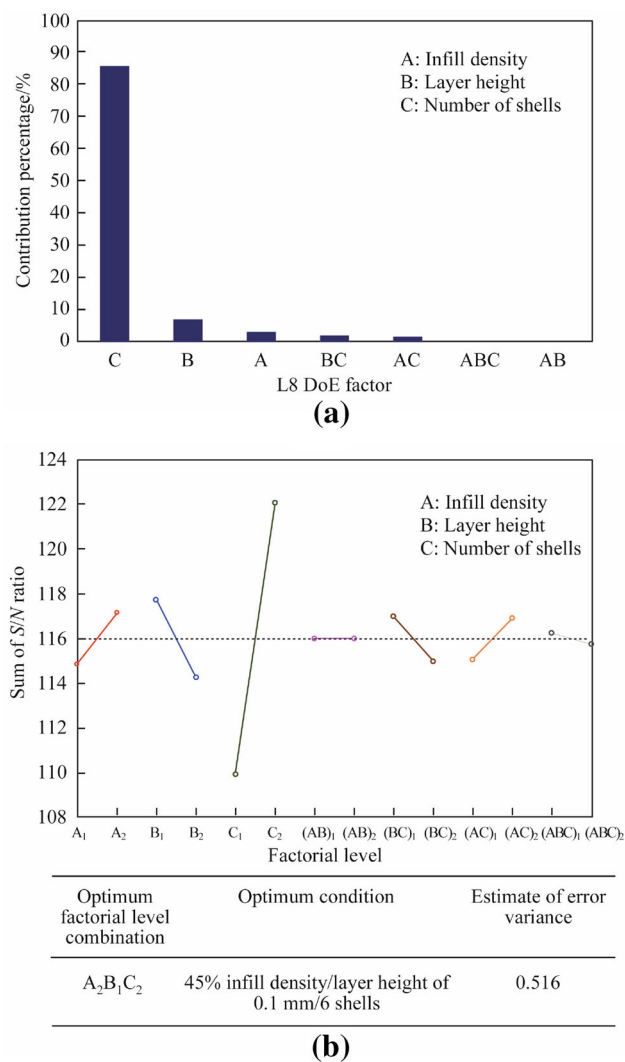


Fig. 2 **a** Pareto ANOVA diagram to identify significant factors in response to maximum tensile strengths of neat PLA testing samples and **b** corresponding sum of S/N ratio diagram

strength measurements for different testing samples due to experimental errors and manufacturing issues.

A simple pareto analysis of variance (ANOVA) [14–16] was utilised to detect significant factors and optimum conditions on the basis of derived cumulative contribution percentage over 85%. With respect to the selection of other non-significant factors, economical and technical requirements were considered accordingly.

5 Results and discussion

5.1 Effect of key processing parameters

The Pareto ANOVA diagram and relevant sum of S/N ratio diagram are illustrated in Figs. 2a, b, respectively, in order

Table 3 DoE factors and levels used for 3D printing neat PLA and PLA/wood fibre composite samples based on material type and number of shells

Factor	Level		
	1	2	3
A': Material type	PLA	PLA/wood fibre composites	
C: Number of shells	2	4	6

Table 4 L_6 DoE orthogonal array for 3D printing neat PLA and PLA/wood fibre composite samples based on material type and number of shells

DoE run	A': Material type	C: Number of shells	A'C
1	1	1	1
2	1	2	2
3	1	3	3
4	2	1	2
5	2	2	1
6	2	3	3

to identify significant factors for the maximum tensile strength of 3D printed PLA testing samples. As evidently depicted in Fig. 2a, the number of shells (factor C) is deemed to be the most significant factor with its contribution percentage of 85.54%, which is followed by layer height (factor B) at 6.99% and infill density (factor A) at 3.04%. However, it appears that the effect of factorial interaction is quite trivial, as evidenced by very small contribution percentages of 2.3% and 1.97% for BC and AC interactions and nearly no contributions from ABC and AB. Consequently, the best combination of factors and levels in this DoE study can be determined as $A_2B_1C_2$, namely 45% infill density, layer height of 0.1 mm and 6 shells, which is solely based upon a mathematically higher sum of S/N ratios, as illustrated in Fig. 2b.

5.2 Effects of the number of shells and material type

In initial aforementioned DoE study, the number of shells is the only significant factor with a cumulative contribution percentage over 85%. As seen from Table 3, it has been thus suggested that further DoE work should be solely based on the number of shells at three levels of 2, 4 and 6 as well as material type (i.e., PLA and PLA/wood fibre composites) as the additional factor while infill density of 15% and layer height of 0.1 mm are fixed for machine default parameters with technical and economical consideration. Such a factorial selection leads to a typical L_6 ($2^1 \times 3^1$) DoE array, also with the consideration of factorial

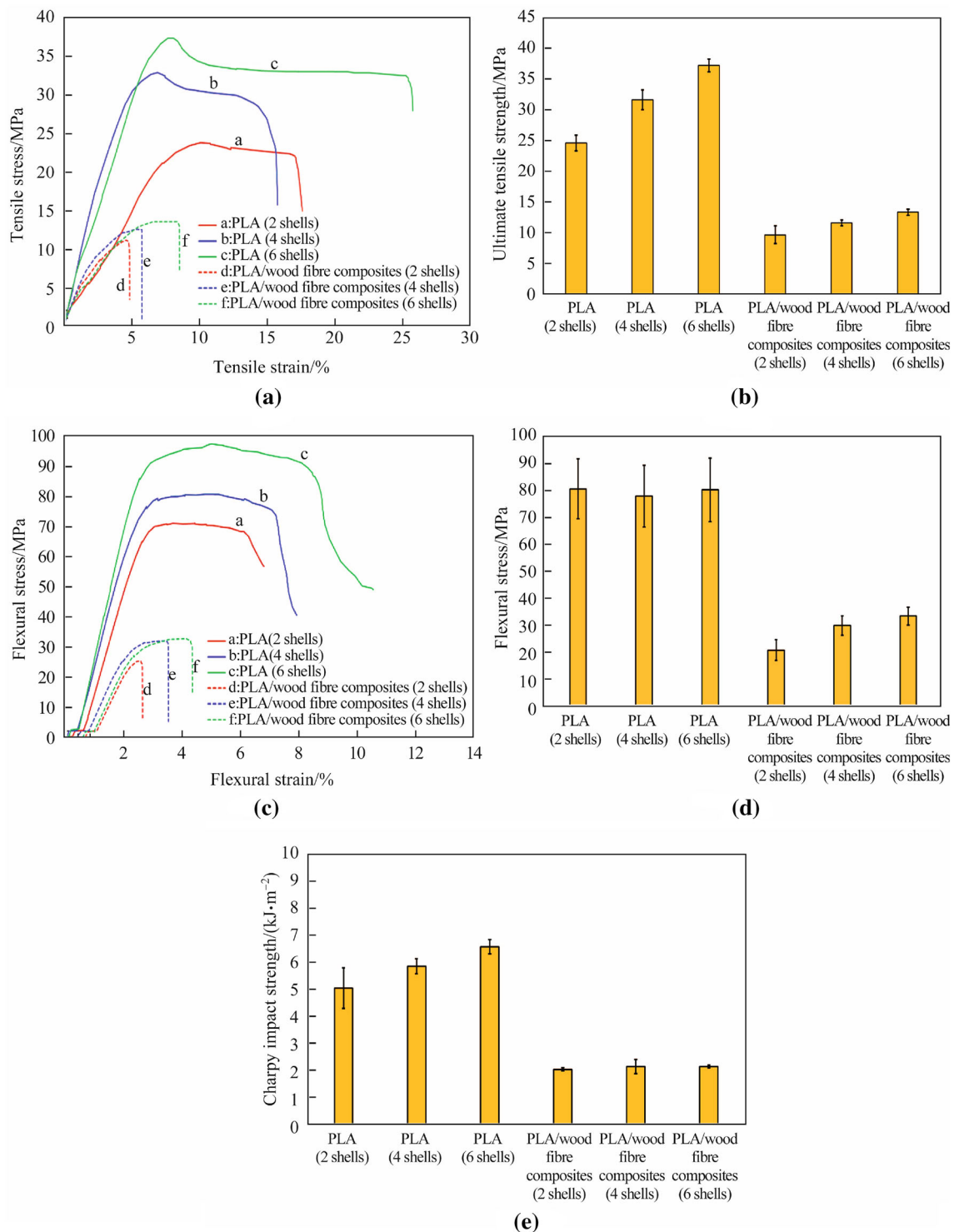
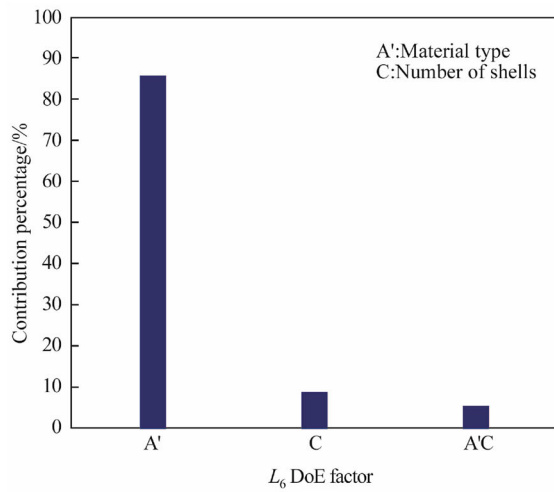


Fig. 3 Mechanical properties of PLA and PLA/wood fibre composite testing samples **a** a typical tensile stress vs. tensile strain curve, **b** ultimate tensile strength, **c** a typical flexural stress vs. flexural strain curve, **d** flexural strength and **e** Charpy impact strength

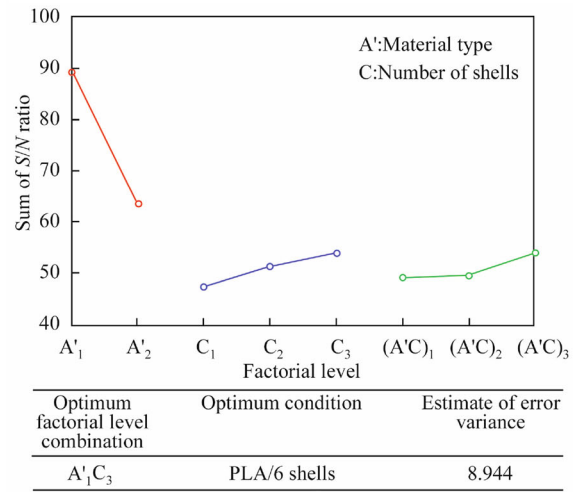
interaction shown in Table 4. In such an array, 6 DoE runs are required for a complete experimental design. Relevant individual DoE responses were set up to be maximum values of tensile strengths, flexural strengths and impact

strengths for testing materials, respectively, in accord with Eq. (1) for the overall evaluation of mechanical strengths.

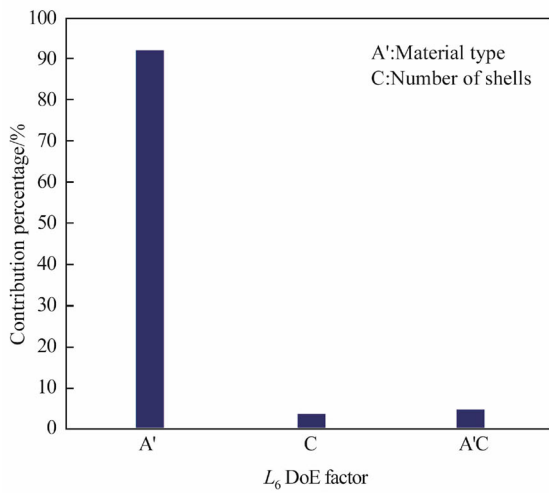
Typical tensile stress vs. tensile strain and flexural stress vs. flexural strain curves are presented in Figs. 3a, c



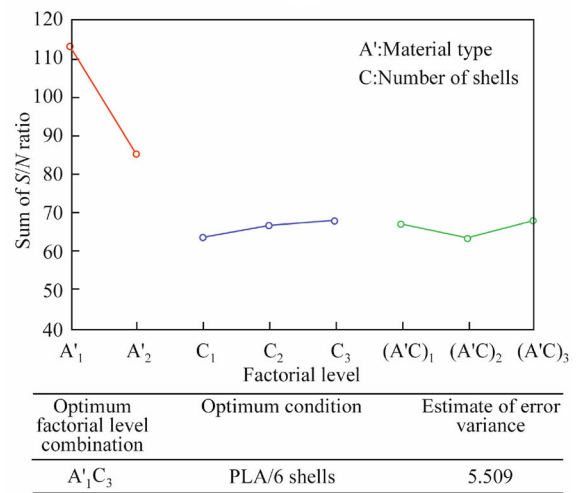
(a)



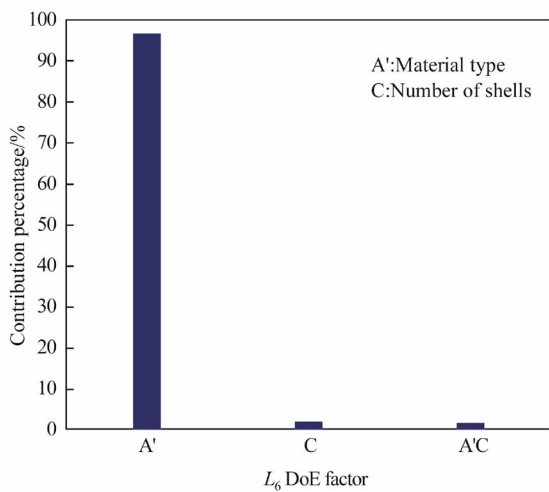
(b)



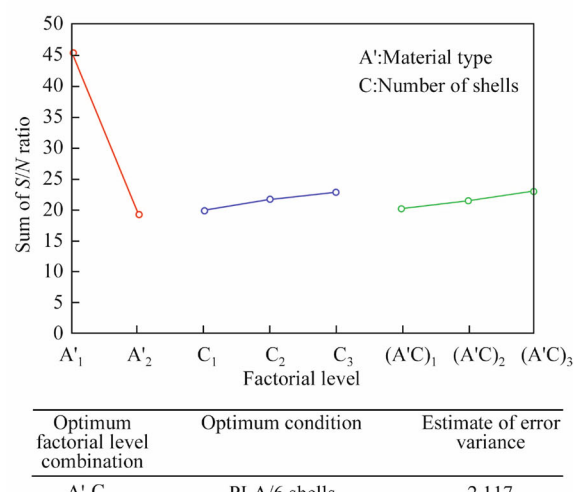
(c)



(d)



(e)



(f)

Fig. 4 Pareto ANOVA diagrams and corresponding sum of S/N ratio diagrams **a** and **b** for tensile testing samples, **c** and **d** for flexural testing samples, and **e** and **f** for impact testing samples, respectively

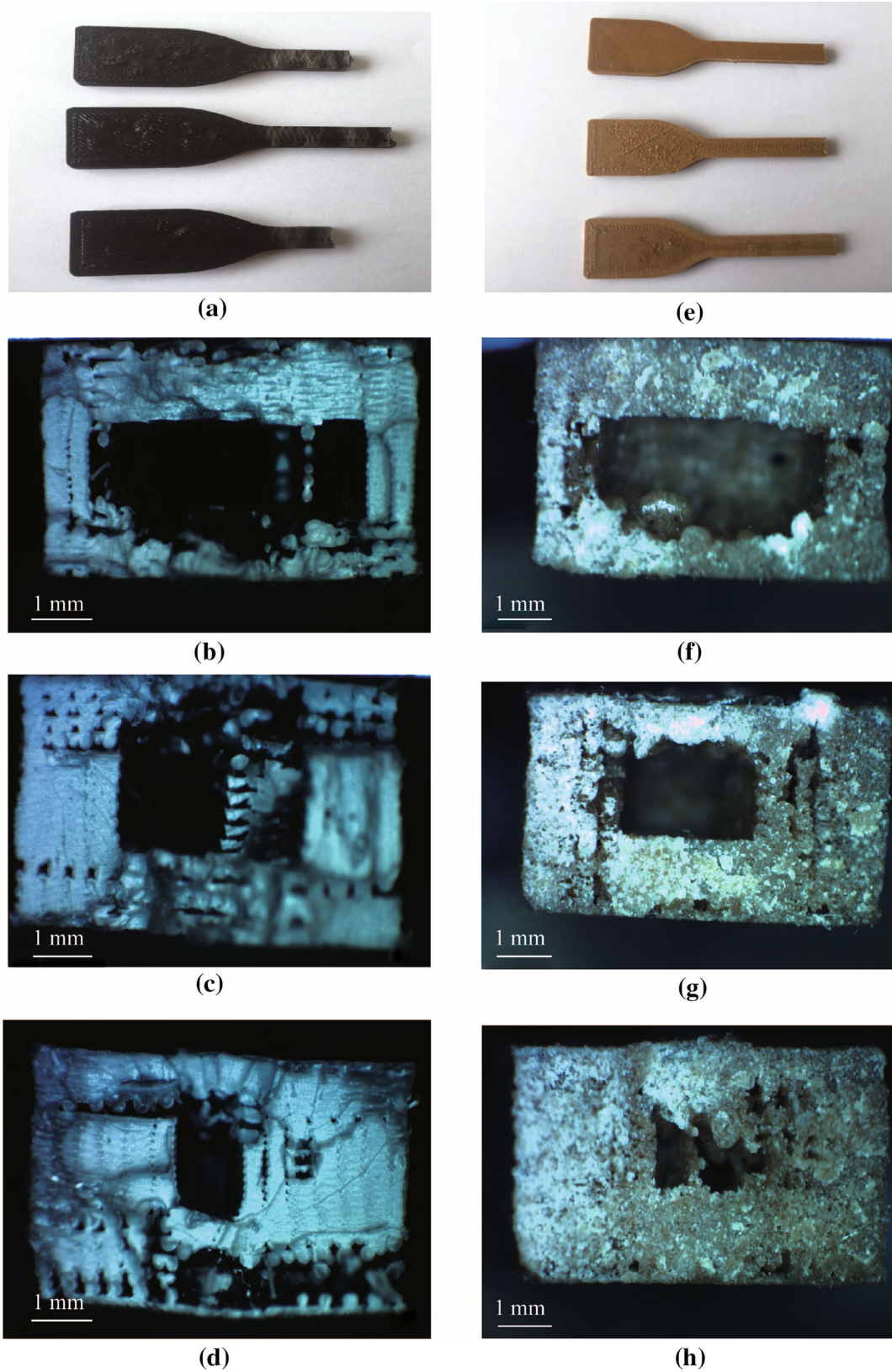


Fig. 5 Ruptured PLA tensile samples **a** top view and typical cross-sectional areas based on **b** 2 shells, **c** 4 shells and **d** 6 shells from the top to the bottom, as well as ruptured PLA/wood fibre composite tensile samples, **e** top view and typical cross-sectional areas based on **f** 2 shells, **g** 4 shells and **h** 6 shells from the top to the bottom

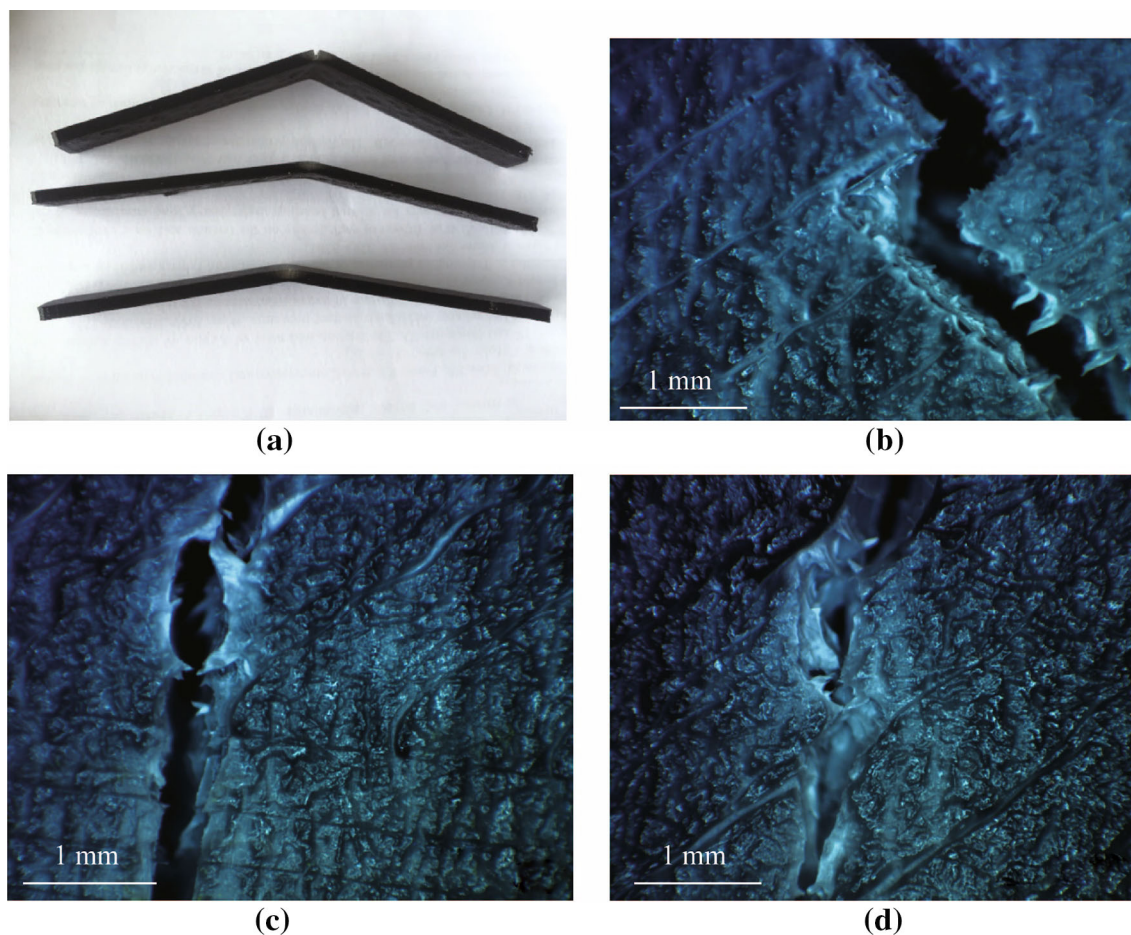


Fig. 6 Ruptured PLA flexural samples (the numbers of shells: 2, 4 and 6 from top to bottom) **a** top view as well as their typical ruptured areas (without full break) **b** 2 shells, **c** 4 shells and **d** 6 shells

PLA and PLA/wood fibre composite samples, along with their reported ultimate tensile strengths, flexural strengths and Charpy impact strengths in Figs. 3b, d, e, respectively. In a consistent manner, all three mechanical strengths of PLA testing samples are much higher than those of PLA/wood fibre composite counterparts. As expected, composite testing samples tend to fracture at small tensile/flexural strains owing to their typical brittle nature when embedded with excessive amounts of wood fibres, as shown in Figs. 3a, c. It is manifested that increasing the number of shells gives rise to the simultaneous enhancements of ultimate tensile strengths and impact strengths for PLA and PLA/wood fibre composite samples despite a much less strength increasing level for the latter. As observed in Fig. 3b, ultimate tensile strengths of PLA samples are improved from 24.79 MPa, 31.80 MPa to 37.38 MPa when the number of shells increases from 2, 4 to 6 as opposed to 9.84 MPa, 11.78 MPa to 13.49 MPa for composite samples, respectively. Furthermore, Charpy impact strengths of PLA samples are 5.06 kJ/m², 5.86 kJ/

m² and 6.59 kJ/m² for 2, 4 and 6 shells in comparison with 2.04 kJ/m², 2.14 kJ/m² and 2.15 kJ/m² for corresponding composite samples. With respect to flexural strengths, though PLA/wood fibre composites still follow a similar strength increasing tendency from 20.41 MPa, 29.54 MPa to 33 MPa with increasing numbers of shells from 2, 4 to 6, flexural strengths of PLA samples remain relatively fluctuating in range from 77.44 MPa to 80.09 MPa. The latter finding may be associated with the fact that PLA samples are not completely broken up to a testing limit (i.e., at 5% flexural strain) in a flexural mode, as depicted in Fig. 3c.

According to Pareto ANOVA diagrams demonstrated in Figs. 4a, c, e, material type (factor A') is clearly shown to have a predominant impact simultaneously on the maximisation of tensile, flexural and impact strengths with contribution percentages of 86.02%, 92.18% and 96.43%, respectively. Nevertheless, contribution percentages for the effects of both the number of shells (factor C) and the interaction A'C are no more than 8.5% in response to all highest mechanical strengths, which signifies that material

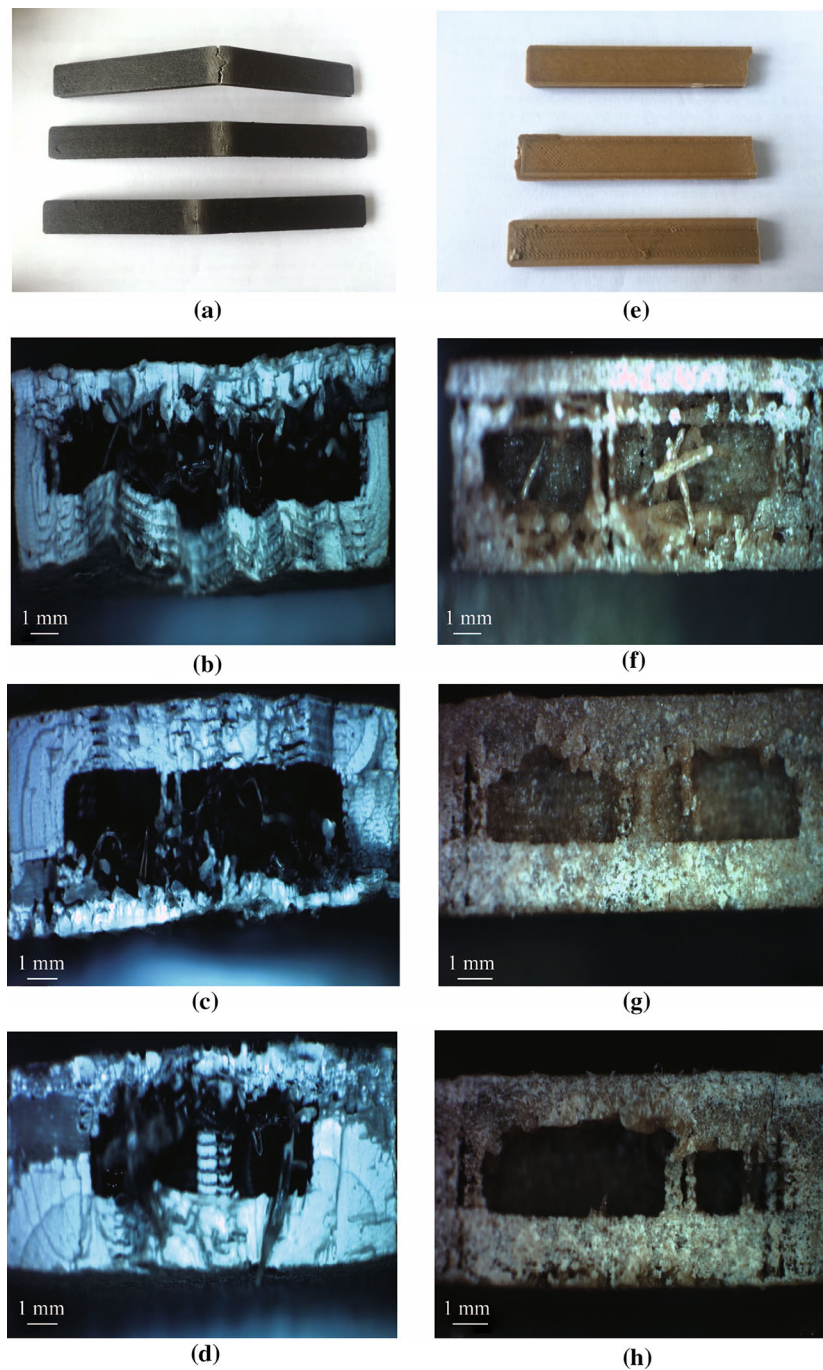


Fig. 7 Ruptured PLA flexural samples **a** top view and typical cross-sectional areas based on **b** 2 shells, **c** 4 shells and **d** 6 shells from the top to the bottom, as well as ruptured PLA/wood fibre composite flexural samples: **e** top view and typical cross-sectional areas based on **f** 2 shells, **g** 4 shells and **h** 6 shells from the top to the bottom

selection may be more critical than actual processing parameters in 3D printing to improve mechanical properties. The corresponding sum of S/N ratio diagrams, illustrated in Figs. 4b, d, f, indicate the same best combination of factors, namely A_1C_3 (to represent the use of neat PLA material with 6 shells) in the 3D printing process regardless of types of mechanical strengths obtained.

5.3 Cross-sectional structures

Figure 5 demonstrates 3D printed cross-sectional structures for PLA and PLA/wood fibre composite tensile samples, respectively. PLA samples contain material strands with a clear sign of typical layer-by-layer structures, which is hardly seen for PLA/wood fibre composite counterparts.

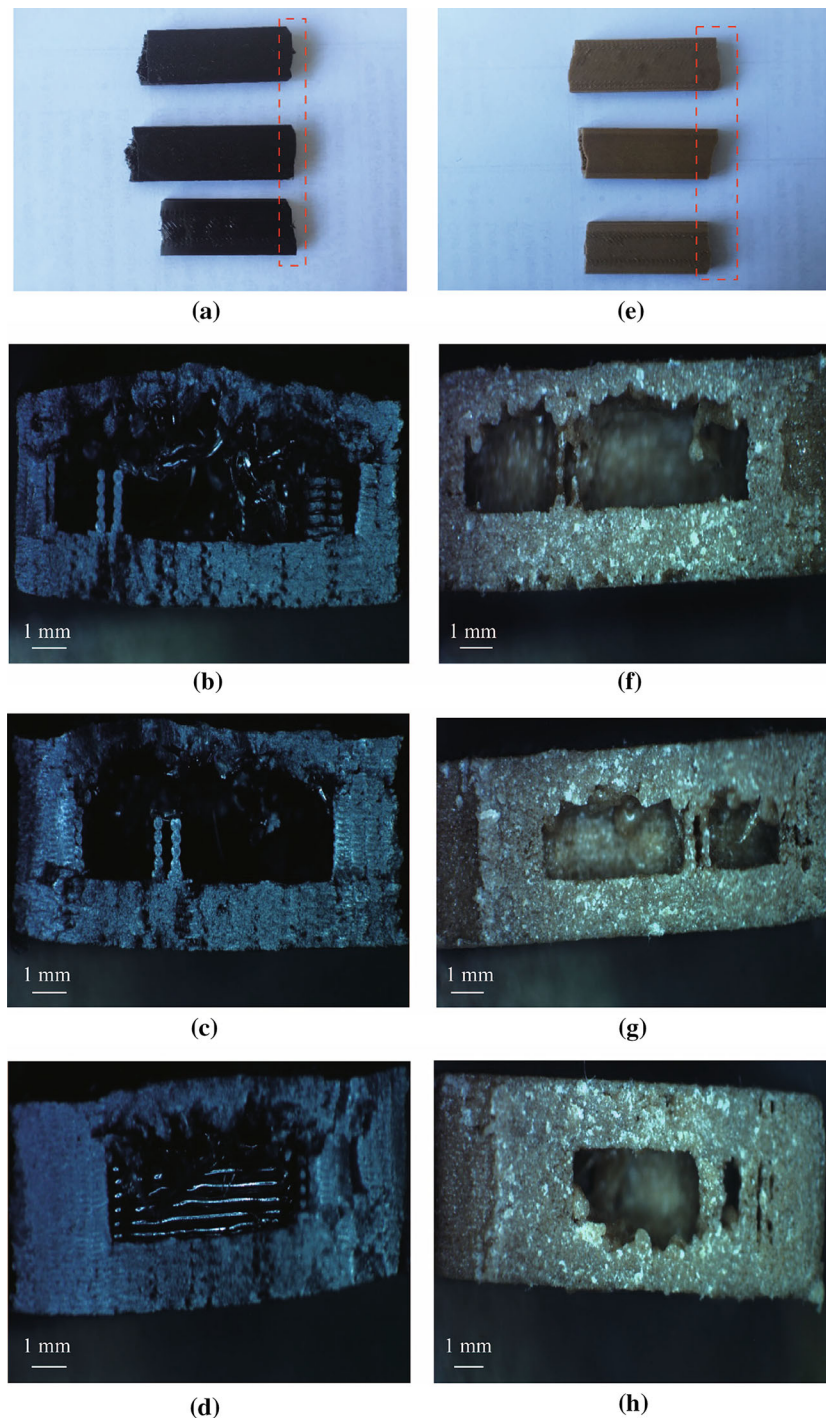


Fig. 8 Ruptured PLA impact samples (the numbers of shells: 2, 4 and 6 from top to bottom) **a** top view (the dash-line block represents broken areas by impact) and their typical ruptured areas **b** 2 shells, **c** 4 shells and **d** 6 shells, as well as ruptured PLA/wood fibre composite impact samples (the numbers of shells: 2, 4 and 6 from top to bottom) **e** top view (the dash-line block represents broken areas by impact) and their typical ruptured areas **f** 2 shells, **g** 4 shells and **h** 6 shells

Instead, abundant randomly oriented wood fibres that are connected loosely occur within ruptured sections of composite samples. Clearly, composite samples possess relatively brittle material characteristic as opposed to neat PLA. Furthermore, an increase in the number of shells is

believed to assist in building up more dense layered structures, particularly for PLA samples, which may partly explain why tensile strengths of PLA samples are superior to those of composite counterparts, as illustrated in Figs. 3a, b. The other plausible reason can be associated

with more non-uniform fibre bundles to cause the weak interfacial bonding between PLA matrices and wood fibres owing to an excessively high fibre content of 60% (weight) within PLA/wood fibre composites.

Figure 6 exhibits ruptured PLA flexural samples without full break and their typical ruptured areas. As observed in Fig. 6a, when the number of shells increased from 2 to 6, PLA samples underwent less significant deflection and break at failure. This phenomenon implies that PLA samples can be bent just that far without fracture and provide a better resistance to hold their strip-like shapes with increasing the number of shells. With a closer look at ruptured areas displayed in Figs. 6b–d, ruptured gaps appear to be reduced in size when the number of shells increases. More interestingly, there exist some noticeable stretched PLA strands near material surfaces and gap regions, clearly indicating typical ductile nature of PLA. On the contrary, flexural samples of PLA/wood fibre composites tend to completely fracture for all batches under this 3-point bending mechanism (see Fig. 7e). Cross-sectional structures in Fig. 7 also suggest strong shell-layered structures for PLA flexural samples as opposed to loose fibre-bundle formations for composites, which is in good accordance with those similar structures detected in tensile samples.

Figure 8 demonstrates cross-sectional structures of PLA and PLA/wood fibre composite samples, respectively. As expected, higher impact energy level is generally required to break PLA samples with strong layer-by-layer structures (see Figs. 8b–d), as compared with corresponding PLA/wood fibre composite samples due to the existence of weakly bound fibre bundles (see Figs. 8f–h). As such, the 3D printed structural formation has played an important role in the variation of Charpy impact strengths shown in Fig. 3e.

Overall, regardless of material type used in this study, it is undoubted that the more number of shells was employed for hierarchical structures, the much higher mechanical strengths could be achieved. As the infill density is predetermined to be 15% according to the second DoE work in Table 3, all material samples inevitably possess single or multiple infill cavities in cross-sectional areas, as depicted in Figs. 5, 7 and 8. However, such infill cavities have been found to be consistently reduced with increasing the number of shells. When strong 3D printed products with high stiffness are not required by the end-users, the decrease in infill density can significantly reduce 3D printing time and material cost in additive manufacturing, thus leading to a high productivity level.

6 Conclusions

3D printed tensile, flexural and impact testing samples of PLA and PLA/wood fibre composites were successfully prepared in this study. The initial L_8 DoE work suggests that the number of shells is the only most significant factor in response to maximum tensile strengths of PLA samples, which is sequentially followed by layer height and infill density. Consistently, further L_6 DoE analysis identifies the sole prevalent impact of material type over the number of shells when maximum tensile, flexural and impact strengths are taken as the DoE responses. Overall, all mechanical strengths of PLA samples have been shown to be much higher than those of their composite counterparts, mainly resulting from closely bound layer-by-layer cross-sectional structures of PLA. Furthermore, excessive amounts of wood fibres within composite samples can result in randomly oriented fibre bundles to cause the weak interfacial bonding between PLA matrices and wood fibres. Finally, an increase in the number of shells tends to improve all mechanical strengths and reduce infill cavities irrespective of material type used.

References

- Chen D, Heyer S, Ibbotson S et al (2015) Direct digital manufacturing: definition, evolution, and sustainability implications. *J Clean Prod* 107:615–625
- Murphy SV, Atala A (2014) 3D bioprinting of tissues and organs. *Nat Biotechnol* 32:773–785
- Gao W, Zhang Y, Ramanujan D et al (2015) The status, challenges, and future of additive manufacturing in engineering. *Comput-Aided Des* 69:65–89
- Li X, Cui R, Sun L et al (2014) 3D-printed biopolymers for tissue engineering application. *Int J Polym Sci* 24:1–13
- Patricio T, Domingos M, Gloria A et al (2013) Characterisation of PCL and PCL/PLA scaffolds for tissue engineering. *Procedia CIRP* 5:110–114
- Senatov FS, Niaza KV, Zadorozhnyy MY et al (2016) Mechanical properties and shape memory effect of 3D-printed PLA-based Porous scaffolds. *J Mech Behav Biomed Mater* 57:139–148
- Rosenzweig DH, Carelli E, Steffen T et al (2015) 3D-printed ABS and PLA scaffolds for cartilage and nucleus pulposus tissue regeneration. *Int J Mol Sci* 16:15118–15135
- Inzana JA, Olvera D, Fuller SM et al (2014) 3D printing of composite calcium phosphate and collagen scaffolds for bone regeneration. *Biomaterials* 35:4026–4034
- Bakarich SE, Gorkin IR, Panhuis MIH et al (2014) Three-dimensional printing fiber reinforced hydrogel composites. *ACS Appl Mater Interfaces* 6:15998–16006
- Le Duigou A, Castro M, Bevan R et al (2016) 3D printing of wood fibre biocomposites: from mechanical to actuation functionality. *Mater Des* 96:106–114
- Suwanprateeb J, Sangam R, Suvannapruk W et al (2009) Mechanical and in vitro performance of apatite-wollastonite glass ceramic reinforced hydroxyapatite composite fabricated by 3D-printing. *J Mater Sci-Mater Med* 20:1281–1289

12. Compton BG, Lewis JA (2014) 3D-printing of lightweight cellular composites. *Adv Mater* 26:5930–5935
13. Richter C, Lipson H (2011) Untethered hovering flapping flight of a 3D-printed mechanical insect. *Artif Life* 17:73–86
14. Park SH (1996) Robust design and analysis for quality engineering. Chapman & Hall, London
15. Dong Y, Bhattacharyya D (2008) Effect of clay type, clay/compatibiliser content and matrix viscosity on the mechanical properties of polypropylene/organoclay nanocomposites. *Compos Part A Appl Sci Manuf* 39:1177–1191
16. Dong Y, Bickford T, Haroosh HJ et al (2013) Multi-response analysis in the material characterisation of electrospun poly (lactic acid)/halloysite nanotube composite fibres based on Taguchi design of experiments: fibre diameter, non-intercalation and nucleation effects. *Appl Phys A Mater Sci Process* 112:747–757